

A semi-analytical solution for the transient temperature field generated by a volumetric heat source developed for the simulation of friction stir welding

T.F. Flint^{a,b,*}, J.A. Francis^{a,b,*}, M.C. Smith^{a,b}

^a Dalton Nuclear Institute, The University of Manchester, Oxford Road, Manchester, UK

^b School of MACE, The University of Manchester, Oxford Road, Manchester, UK



ARTICLE INFO

Keywords:

Friction stir welding
Green's function
Heat flux model
Thermal analysis
Time dependent heating rate
3D thermal analytical solution

ABSTRACT

The accurate prediction of transient temperature fields, induced in alloy systems during advanced manufacturing processes, is critical. These fields influence the magnitude and distribution of residual stresses, the evolution of material microstructures, and material properties such as fracture toughness. Such predictions in the vicinity of a concentrated heat source require precise knowledge of the associated heat flux as a function of position and time. If the applied thermal load is time-dependent this can have a significant effect on the resulting temperature fields and microstructures. In this work a novel three-dimensional heat source is proposed to represent the friction stir welding process along with the semi-analytical solution for the temperature field. The volumetric heat source model has a nontrivial spatial distribution constructed from physical arguments and may account for complex mass transfer, and the associated thermal effects, without explicitly solving the flow equations. A method for incorporating a time-dependent heating scenario into analytical solutions generated by this heat source is also presented. Predicted temperatures are compared with those measured experimentally for two cases reported in the literature and good agreement is observed. Example solutions for various time-dependent heat inputs are also presented.

1. Introduction and background

When compared to fusion welding processes, the friction stir welding (FSW) of aerospace alloys often leads to improvements in weldability and joint performance. FSW has also found application in the nuclear sector for the sealing of nuclear waste containers [1–3]. FSW joins materials via mechanical intermixing across the joint through pressure and torque applied through the FSW tool, that causes heating and plastic deformation. During FSW the substrate material does not experience melting, as would be the case in fusion welding processes. The relatively low peak temperatures, and avoidance of problems associated with state change such as porosity, inclusions, solute redistribution and solidification cracking, can lead to improved mechanical properties [4–6]. FSW is performed using a non-consumable rotating tool with a specially designed shoulder and pin; this tool is lowered into the seam between two abutting plates until the shoulder rests on the top surface, as shown in Fig. 1. After an initial dwell period as the tool is lowered into the work-piece the tool traverses along the seam between the two plates [7–9].

The friction stir welding process is divided into three discrete events, these being the dwell period at the start of the weld, the traverse

period as the tool moves and the dwell period at the end of the weld as the tool stops and is extracted [4,10]. The rotating tool produces heat via friction between the tool and the work-piece and moves the material in its vicinity to produce the joint [11,12]. The heating is accomplished by friction between the tool and the work-piece and plastic deformation of work-piece [13]. The localised heating softens the material around the pin and a combination of tool rotation and translation leads to movement of material from the front of the pin to the back of the pin. The primary source of heat generation is friction between the shoulder of the tool and the plates being joined [14]. The pin's primary function is to induce flow of the material around the tool, while the generation of heat is a secondary function [15].

The first step in predicting the mechanical properties of a weld is to predict the complex thermal field resulting from the application of the FSW tool [16,17]. 3D heat transfer models with constant heat flux input from the tool interface have been utilised and used the finite element method to solve for the transient temperature field in the tool and work-piece [9,18]. Models for the heat input to the work-piece from the FSW tool have been developed, based on assumptions in relation to the contact condition between the rotating tool surface and the weld piece [19]. The limitations of such surface flux based models are twofold;

* Corresponding authors. Dalton Nuclear Institute, The University Of Manchester, Oxford Road, Manchester, UK.

E-mail addresses: Thomas.Flint@manchester.ac.uk (T.F. Flint), John.Francis@manchester.ac.uk (J.A. Francis).

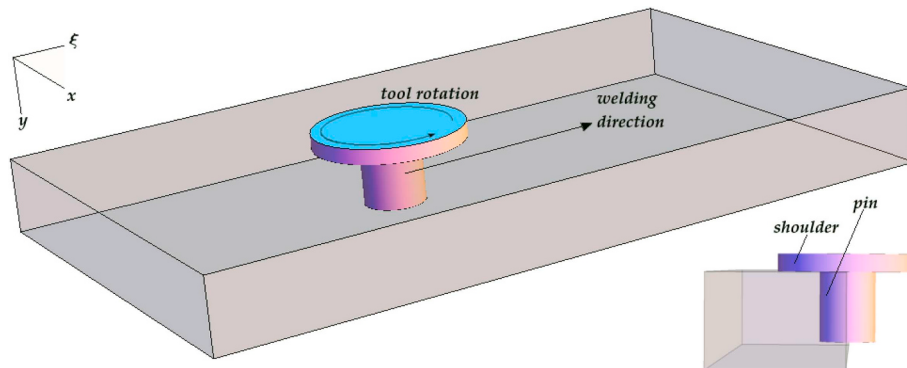


Fig. 1. Pin and Shoulder Arrangement in the FSW process.

firstly the flow of material around the tool has the effect of distributing the heat in some manner and secondly the total heat input is a function of the dimensionless slip rate that is itself temperature dependent [20]. Surface flux based heating approaches may be overcome, by including the underlying physics in a coupled computational fluid dynamics (CFD) model. These CFD models fully account for the complex flow dynamics and coupled heat transfer around the tool, namely the material flow producing heat generation by plastic dissipation in the shear layer and frictional contact at the interface between the tool and workpiece [5,7,11,14,15,21]. CFD simulations of FSW more accurately capture the physical mechanisms driving the thermal and subsequent microstructural changes within the substrate material. These CFD approaches have been shown to generate the most accurate thermo-mechanical fields of any simulation procedure, however they are extremely computationally expensive [21–23]. Due to the large computational cost of CFD modelling approaches there is a desire for novel and efficient analytical techniques for the solution of heat transfer problems applied to representative problems.

Recently a novel transient analytical solution based on the Green's function method was established to obtain the 3D thermal field by considering the FSW tool as a simplified circular heat source moving in a finite rectangular plate [24]; this Green's function approach permits the transient temperature field induced in the component to be computed analytically, free from numerical discretisation errors, as the geometry of a friction stir weld is orthogonal. In the case of FSW, the analytical solution is not an approximation but an optimisation of the solution procedure [24,25]. Similar analytical solution techniques have been shown to accurately predict the temperature field generated in a component subjected to an electron beam (EB) welding process with extremely high accuracy [26]. In the literature the terms analytical solution and semi-analytical solution are often used interchangeably. This is due to the fact that the final temporal integral has no closed form analytical solution and so is computed numerically. In these analytical thermal solution approaches, often the only simplification is the assumption of constant thermal properties. It has been shown by Zhu et al. that assuming constant thermal properties does not lead to significant decreases in accuracy when compared to simulations incorporating temperature dependent thermal properties [27].

In thermal solution procedures where the flow effects are not explicitly modelled, some accounting for the distribution effect of the heat should be made [28]. The distribution of this heat around the tool should be carefully considered. The peak value of heat distribution may also vary in time, due to the fact that the slip rate and coefficient of dynamic friction are temperature dependent [18]. It is advantageous to include a time-dependent heat flux, with a volumetric heat distribution representative of the heat transfer to the domain from the FSW tool, to capture the complex thermal fields generated during the process.

In the present work a new method for incorporating time dependent heat input into the analytical solution for the induced transient temperature field in a finite computational domain due to the application of

a new volumetric heat source is outlined. A new representation for the heat source in the FSW process is presented in conjunction with the analytical solution for the temperature field. The proposed heat source model aims to address deficiencies in current heat source descriptions, for cases where material motion around the FSW tool is neglected. The goal is to generate a thermal solution to the FSW process that captures the complex heat and mass transfer around the tool, using a novel heat source description, without explicitly solving the complex flow equations, in a computationally efficient manner. For the first time representative examples of time dependent heat input are outlined and solved analytically to highlight the flexibility of the solutions.

2. Proposed volumetric heat source for the friction stir welding process

The temperature of the domain, $T_{(x,y,z,t)}$, as a function of spatial coordinates, (x, y, z) , and time, t , satisfies Equation (1) when mass transfer within the domain is neglected.

$$\rho c_p \frac{\partial T}{\partial t} - k \nabla^2 T = q \quad (1)$$

Here ρ , c_p and k are the mass density, specific heat capacity and the thermal conductivity respectively; $q_{(x,y,z,t)}$ is the rate of internal heat generation. The importance of an adequate model for the weld heat source, $q_{(x,y,z,t)}$, in the analysis of the thermal cycle has been emphasised by several investigators in the case of fusion welding [29–31]. If a volumetric flux distribution is proposed, the form of the distribution should be scrutinised [13]. Consider a cylinder rotating in a thermally conducting domain, generating heat due to friction between the cylinder surface and the domain. If a path were taken through the body of the cylinder, two maxima in heat would be expected, corresponding to the locations at which the path enters and exits the cylinder. Outside the surface of the cylinder one would expect the heat generation rate to decrease in some manner; also as the centre of the cylinder is not in contact with the domain one should expect the heat generation at the centre of the rotating cylinder to decrease to a minimum also. On a path taken vertically through the body of the cylinder, some small distance from the curved surface in contact with the domain, one would expect the heat generation to be constant until the base of the cylinder were reached. At the base of the cylinder one would expect the heat generation rate to decay in some manner with increasing distance from the end of the cylinder. If these assumptions regarding the behaviour of the heat flux distribution are applied, a volumetric heat flux distribution may be found to satisfy all conditions.

In order to construct a volumetric heat source with the desired characteristics, consider a Cartesian domain (z, y, ξ) separated into four quadrants by planes at $y = d_g$ and $\xi = 0$. The $y = d_g$ plane is analogous with the base of the rotating cylinder. Another plane is selected as an analogy for the initiation point of the rotating cylinder at $y = y_i$, this will be used as an integration limit during the derivation of the heat

source model; $d_g - y_i$ is therefore the depth of the rotating cylinder. The transformation relating the fixed (x, y, z) and the moving (x, y, ξ) coordinate system is $\xi = z - vt$ where v is the travel velocity of the tool. As a distribution of heat through the ξ and x directions is sought, with two maxima and a minima at the origin, which decays in some non-linear manner is sought; a distribution that is the difference of two bivariate Gaussian distributions is chosen to satisfy the form of the distribution. Below the base of the cylinder, ($y_i \geq d_g$), there is an additional dependency on the depth coordinate to ensure the heat generation rate decreases as the distance from the base of the cylinder decreases. Above the base of the cylinder, ($y_i < y \leq d_g$), the heat generation rate does not depend on depth assuming the cylinder has a constant radius. The locations of the maxima, ahead and trailing the origin in the ξ coordinate, were not limited to the same value [31]. The quadrants of the distribution must then be matched at the region boundaries, the details of which are shown in Appendix A, in order to find the final form of the volumetric distribution as shown in Equation (2). Fig. 2 shows surfaces of constant power density generated by the heat source model.

$$q = Q_{(t)} \cdot \begin{cases} \frac{R_2 2 \sqrt{3} \Gamma}{b c_r \pi^2} \begin{cases} e^{-3 \left[\left(\frac{x-b_g}{\frac{\pi a}{3k_p}} \right)^2 + \left(\frac{y-d_g}{b} \right)^2 + \left(\frac{\xi}{\frac{\pi c_f}{3k_p}} \right)^2 \right]} \\ -e^{-3 \left[\left(\frac{x-b_g}{\frac{a}{k_p}} \right)^2 + \left(\frac{y-d_g}{b} \right)^2 + \left(\frac{\xi}{\frac{c_f}{k_p}} \right)^2 \right]} \end{cases} & \forall x, y \geq d_g, \xi \leq 0 \\ \frac{R_1 2 \sqrt{3} \Gamma}{b c_f \pi^2} \begin{cases} e^{-3 \left[\left(\frac{x-b_g}{\frac{\pi a}{3k_p}} \right)^2 + \left(\frac{y-d_g}{b} \right)^2 + \left(\frac{\xi}{\frac{\pi c_f}{3k_p}} \right)^2 \right]} \\ -e^{-3 \left[\left(\frac{x-b_g}{\frac{a}{k_p}} \right)^2 + \left(\frac{y-d_g}{b} \right)^2 + \left(\frac{\xi}{\frac{c_f}{k_p}} \right)^2 \right]} \end{cases} & \forall x, y \geq d_g, \xi \geq 0 \\ \frac{R_4 \Gamma}{c_f \pi (d_g - y_i)} \begin{cases} e^{-3 \left[\left(\frac{x-b_g}{\frac{\pi a}{3k_p}} \right)^2 + \left(\frac{\xi}{\frac{\pi c_f}{3k_p}} \right)^2 \right]} \\ -e^{-3 \left[\left(\frac{x-b_g}{\frac{a}{k_p}} \right)^2 + \left(\frac{\xi}{\frac{c_f}{k_p}} \right)^2 \right]} \end{cases} & \forall (x, y \leq d_g, \xi \leq 0) \\ \frac{R_3 \Gamma}{c_f \pi (d_g - y_i)} \begin{cases} e^{-3 \left[\left(\frac{x-b_g}{\frac{\pi a}{3k_p}} \right)^2 + \left(\frac{\xi}{\frac{\pi c_f}{3k_p}} \right)^2 \right]} \\ -e^{-3 \left[\left(\frac{x-b_g}{\frac{a}{k_p}} \right)^2 + \left(\frac{\xi}{\frac{c_f}{k_p}} \right)^2 \right]} \end{cases} & \forall (x, y \leq d_g, \xi \geq 0) \\ 0 & \forall (y < y_i) \end{cases} \quad (2)$$

where $Q = \eta P f$ and is the total energy input into the material. In this approach P may be viewed as the total power delivered to the tool and η represents the heat transfer efficiency between the tool and the substrate material. It may be desirable to apply two of these proposed FSW heat source distributions, one for the shoulder and pin respectively. In this case, to ensure energy is not created in the formulation, $f_{pin} + f_{shoulder} = 1$ and f represents the respective fractional heat allocated to the pin and shoulder from the two distributions. $\eta_{(t)}$ can be constant, or vary with time, to account for changes in rotational speed and the dwell periods at the start and end of the FSW process. $\Gamma = 54 k_p^2/a (\pi^2 - 9)$ and k_p is an irrational constant that arises in the derivation of the heat source model as discussed in the appendix and has a value of $\frac{\pi}{3} \sqrt{\ln \left[\frac{\pi^2}{9} \right] / \sqrt{3 \left(\frac{\pi^2}{9} \right)}} - 3 \approx 0.59071$. The parameters a, b, c_r and c_f are the heat flux parameters that determine the spatial gradient of the heat flux in the x, y and ξ directions respectively. The parameter b_g is the location of the heat source along the x -axis. The

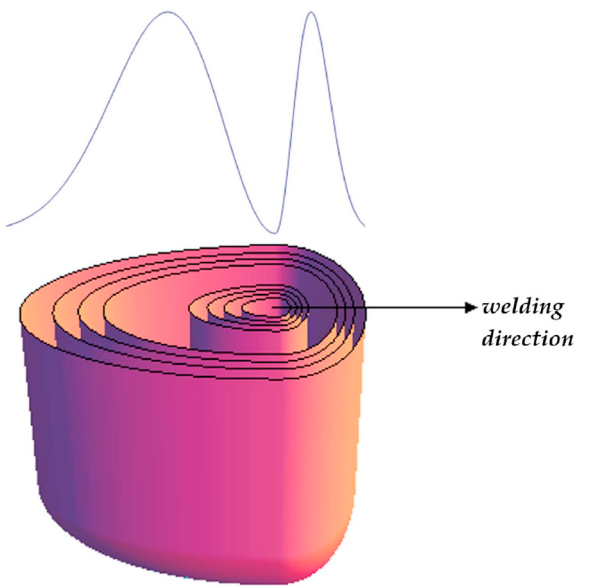


Fig. 2. Flux Distribution due to a travelling rotating cylinder showing relative flux magnitude.

efficiency is itself a function of time, $\eta(t)$, as the power transferred to the work piece is not constant. The fitting parameters denoted by R_1, R_2, R_3 and R_4 are found by matching the flux distributions at the origin in the moving reference frame and are given by:

$$\begin{aligned} R_1 &= \frac{b c_f}{(c_f + c_r) \left(b + 2 \sqrt{\frac{3}{\pi} (d_g - y_i)} \right)} \\ R_2 &= \frac{b c_r}{(c_f + c_r) \left(b + 2 \sqrt{\frac{3}{\pi} (d_g - y_i)} \right)} \\ R_3 &= \frac{6 c_f (d_g - y_i)}{(c_f + c_r) (6(d_g - y_i) + b \sqrt{3\pi})} \\ R_4 &= \frac{6 c_r (d_g - y_i)}{(c_f + c_r) (6(d_g - y_i) + b \sqrt{3\pi})} \end{aligned}$$

3. Semi-analytical solution procedure

The semi-analytical solution procedure used in the present work has been fully described for orthogonal geometries, with a combination of insulating and fixed temperature boundary conditions, elsewhere [26]; The deviation from this work in the presented scheme is that the heat input rate is permitted to be a function of time and taken inside the final temporal integral. Consider an orthogonal domain with dimensions of B, D and L in the x, y and z directions, respectively. The one dimensional (1D) Green's function for insulating boundary conditions ($\partial G / \partial x = 0$, at $x = 0$ and $x = B$) is given by Equation (3) [32].

$$G_{(x,x',t,t')} = \sum_{n=-\infty}^{\infty} \frac{\left(\text{Exp} \left[-\frac{((2nB) + x - x')^2}{4\alpha(t - t')} \right] + \text{Exp} \left[-\frac{((2nB) + x + x')^2}{4\alpha(t - t')} \right] \right)}{\sqrt{4\pi\alpha(t - t')}} \quad (3)$$

where $\alpha = k/\rho c_p$ is the thermal diffusivity, ρ is the mass density, k the thermal conductivity and c_p the specific heat of the substrate material. In Cartesian coordinates 1D Green's functions may be multiplied together to find the 3D Green's function for the domain. For a 3D domain with insulating boundary conditions on all faces, the Green's function is given in equation (4).

$$G_{(x,x',y,y',z,z',t,t')} = \sum_{n=-\infty}^{\infty} \left\{ \frac{\left(\text{Exp} \left[-\frac{((2nB)+x-x')^2}{4\alpha(t-t')} \right] + \text{Exp} \left[-\frac{((2nB)+x+x')^2}{4\alpha(t-t')} \right] \right)}{\sqrt{4\pi\alpha(t-t')}} \times \right. \\ \left. \frac{\left(\text{Exp} \left[-\frac{((2nD)+y-y')^2}{4\alpha(t-t')} \right] + \text{Exp} \left[-\frac{((2nD)+y+y')^2}{4\alpha(t-t')} \right] \right)}{\sqrt{4\pi\alpha(t-t')}} \times \right. \\ \left. \left(\text{Exp} \left[-\frac{((2nL)+z-z')^2}{4\alpha(t-t')} \right] + \text{Exp} \left[-\frac{((2nL)+z+z')^2}{4\alpha(t-t')} \right] \right) \right\} \quad (4)$$

Equation (4) gives the temperature increment at point (x, y, z) and instant t due to an instantaneous unit heat source applied at (x', y', z', t') . The temperature variation induced at (x, y, z, t) by an instantaneous heat source of magnitude $q_{(x',y',z',t')}$ is $\frac{1}{\rho c_p} q_{(x',y',z',t')} G_{(x,x',y,y',z,z',t,t')}$. The temperature increment at point (x, y, z, t) is given by equation (5).

$$(\rho c_p)^{-1} \times \int_0^t q_{(x',y',z',t')} G_{(x,x',y,y',z,z',t,t')} dt' \quad (5)$$

Therefore the temperature increment at any point (x, y, z) and time t due to a distributed heat source $q_{(x',y',z',t')}$ for an orthogonal domain with insulating boundary conditions on all surfaces is given by equation (6)

$$\Delta T(x, y, z, t) = \int_0^t \int_0^L \int_0^D \int_0^B q_{(x',y',z',t')} G_{(x,x',y,y',z,z',t,t')} dx' dy' dz' dt' \quad (6)$$

Due to the orthogonality present in the joint geometry in FSW the multiplication of one dimensional Green's functions yields a three dimensional Green's function that is representative of the problem. The temperature $T_{(x,y,z,t)}$ for any point in the domain, due to the proposed volumetric heat source, is then given by Equation (7) where G_X , G_Y and G_Z represent the one dimensional Green's functions in the x , y and z dimensions respectively.

$$\Delta T = \frac{Pf}{\rho c_p} \int_0^t \eta_{(t')} \left\{ \left[\frac{R_1 2 \sqrt{3} \Gamma}{b c_f \pi^{\frac{3}{2}}} \left(I_f \int_{d_g}^D G_Y e^{-3\left(\frac{y'-d_g}{b}\right)^2} dy' \right) \right] \right. \\ \left. + \left[\frac{R_2 2 \sqrt{3} \Gamma}{b c_r \pi^{\frac{3}{2}}} \left(I_r \int_{d_g}^D G_Y e^{-3\left(\frac{y'-d_g}{b}\right)^2} dy' \right) \right] \right\} dt' \\ + \left[\frac{R_3 \Gamma}{c_f \pi (d_g - y_l)} \left(I_f \int_{y_l}^{d_g} G_Y dy' \right) \right] \\ + \left[\frac{R_4 \Gamma}{c_r \pi (d_g - y_l)} \left(I_r \int_{y_l}^{d_g} G_Y dy' \right) \right] \quad (7)$$

where I_f and I_r are given in Equations (8) and (9) respectively.

$$I_f = \int_0^B G_X e^{-3\left(\frac{(x'-b_g)^2}{\left(\frac{\pi a}{3k_p}\right)^2}\right)} dx' \int_{vt'}^L G_Z e^{-3\left(\frac{(z'-vt')^2}{\left(\frac{\pi c_f}{3k_p}\right)^2}\right)} dz' \\ - \int_0^B G_X e^{-3\left(\frac{(x'-b_g)^2}{\left(\frac{a}{k_p}\right)^2}\right)} \int_{vt'}^L G_Z e^{-3\left(\frac{(z'-vt')^2}{\left(\frac{c_f}{k_p}\right)^2}\right)} dz' \quad (8)$$

$$I_r = \int_0^B G_X e^{-3\left(\frac{(x'-b_g)^2}{\left(\frac{\pi a}{3k_p}\right)^2}\right)} dx' \int_0^{vt'} G_Z e^{-3\left(\frac{(z'-vt')^2}{\left(\frac{\pi c_r}{3k_p}\right)^2}\right)} dz' \\ - \int_0^B G_X e^{-3\left(\frac{(x'-b_g)^2}{\left(\frac{a}{k_p}\right)^2}\right)} \int_0^{vt'} G_Z e^{-3\left(\frac{(z'-vt')^2}{\left(\frac{c_r}{k_p}\right)^2}\right)} dz' \quad (9)$$

Note that for the dwell periods of the heat source the vt' term is replaced with the l_g term as the heat source is stationary in the dwell

periods of the weld, such that the z -component of the exponent is $z' - l_g$, where l_g is the heat source location along the z -axis.

In Equation (7) the heat input rate, $Q = \eta Pf$, is assumed to be a function of time, as $\eta_{(t')}$, therefore this term is taken inside the temporal integral, as shown in Equation (7). This time integral is computed numerically. This presents a very powerful tool with which to compute the transient thermal field induced in a finite domain due to some inconsistent heat input such as pulsing of the heat source or a sudden termination of the heat input which may represent a loss of power during the welding process. Coupling this with the analytical solution technique ensures any calculations performed are computationally efficient. An example of the type of efficiency distribution that may be used to account for non-linear increases and decreases in heat input is shown in Fig. 3 [33].

4. Application of the method

To demonstrate the flexibility of the distributed heat source model, the analytical solution method, and the versatility of the time varying heat transfer efficiency two cases are considered; the predicted temperature field is then compared with that found experimentally for two cases of FSW of aluminium in the literature. In the first application the heat transfer efficiency, $\eta_{(t)}$, is increased and decreased while the tool is in the stationary dwell periods at the beginning and end of the welding process respectively. In the second application $\eta_{(t)}$ is varied between 0% and 100% in a sinusoidal manner. In both applications a cuboid domain of length 100 mm, depth 20 mm and width 170 mm is considered. The heat source is considered to travel down the centre of the region at x85 mm.

4.1. Ramp up and ramp down

In this example application the heat source is inserted into the domain 25 mm along the z -axis, $l_g = 25$ mm. The efficiency term is then increased from 0% to 100% over 10s for arbitrary maximum heat input rates. Thermal properties of steel are used arbitrarily. After 12.5s the heat source begins to travel with a velocity of 2mm^{-1} for 25s before stopping at $l_g = 75\text{mm}$ for 10s and having the input power decreased to 0% to simulate the extraction of the tool from the work-piece. Fig. 4 shows a cross section along the welding line for various instants in time throughout the simulation.

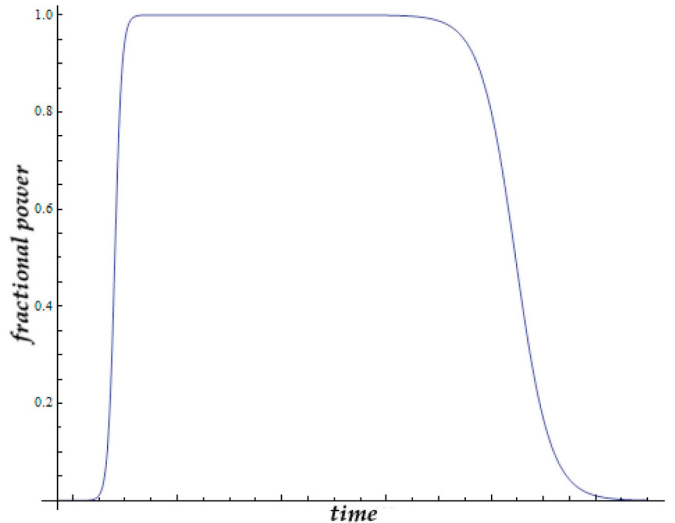


Fig. 3. Input power efficiency as a function of time; accounting for the increase and decrease in rotational velocity and frictional changes as the region around the tool changes temperature.

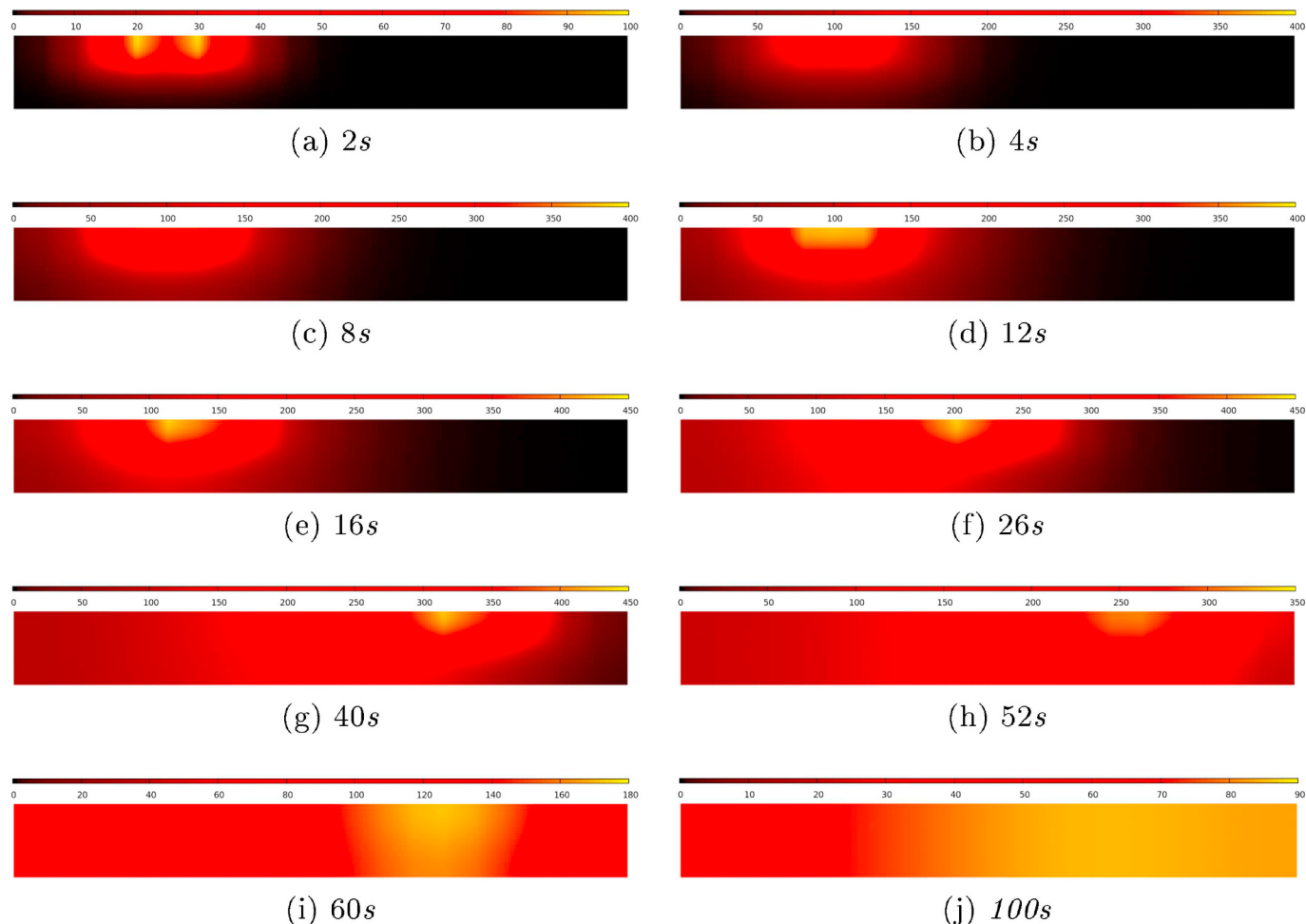


Fig. 4. Cross section through the computational domain at the welding joint showing the thermal response due to the volumetric FSW heat source flux distribution.

4.2. Sinusoidal varying heat input rate

In this application, the time varying heat transfer rate is varied in a sinusoidal manner, for an arbitrary peak power, with a period of 4s as shown in Fig. 5. The heat source parameters used in this case are shown in Table 1 where all parameters have units of mm unless stated otherwise.

The thermal response of the computational domain is shown in Fig. 6; the thermal response is shown as a cross section along the welding line for various instants in time.

It is clear from Fig. 6 that the sinusoidal heat input rate has a clear and defined effect on the analytically computed temperature field, as one might expect, with the peak temperature pulses occurring at the same frequency as the heat source pulses, with some phase shift in time due to the time required for thermal conduction.

4.3. Validation against literature

Experimental validation data is not available, first-hand, to the authors. Results have been compared with the work of Chao et al. in order to ensure a general agreement is reached [34]. In the studied literature friction stir welding was performed between two aluminium plates with a steel tool. Two cases are presented in this study for two different welding travel velocities; the hot weld has a travel velocity of 2.36 mm s^{-1} and the cold weld has a travel velocity of 3.32 mm s^{-1} , both welds are performed with a tool rotational speed of 4 revolutions per second. The hot and cold terminology is chosen by Chao representing the relative heat inputs to the work-piece. Both welds were performed

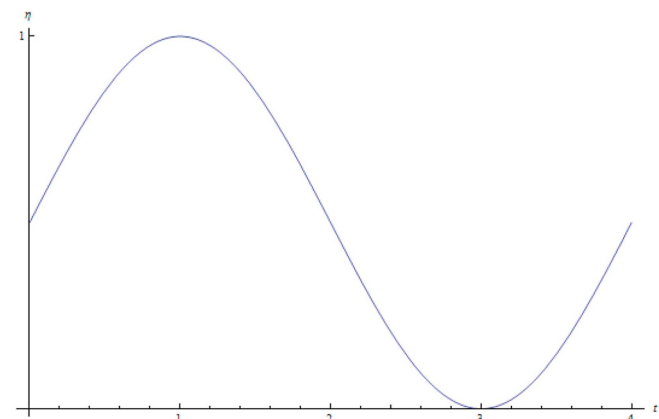


Fig. 5. Sinusoidal variation in the heat transfer efficiency between the heat source and computational domain.

along the centre line of samples with identical geometries. The values of B , D and L are 204 mm , 8.13 mm and 610 mm respectively and $b_g = 102 \text{ mm}$. In the work of Chao et al. an array of 9 thermocouples was placed at locations within the weld geometry and on the surface. The thermocouples that experience the greatest sensitivity to the applied heat flux from the FSW tool are clearly those closest to the welding location, for the experiment these thermocouple locations are 5 mm from the centre line at varying depths. The coordinates of the three closest thermocouples are $(107, 2, 295.5)$, $(107, 4, 305)$ and $(107, D, 314.5)$ referred to as TC_{top} , TC_{middle} and TC_{bottom} respectively. The

Table 1

Heat source parameters for the periodically varying heat transfer to the computational domain.

Parameter	a	b	c_r	c_f	y_i	d_g	b_g	η^a	v^b
Value	5	2	6	4	0	8	85	$\frac{1}{2} + \frac{1}{2}\sin\left(\frac{2\pi}{4}t'\right)$	5

^a Heat transfer efficiency is dimensionless.

^b Units of velocity are $mm\ s^{-1}$

thermal properties of the *AlliCu* alloy used were taken from the literature as $\rho = 2712 \times 10^{-9} kg\ mm^{-3}$, $k = 0.0205 W\ mm^{-1}\ K^{-1}$ and $c_p = 910 J\ kg^{-1}\ K^{-1}$ respectively.

To demonstrate the functionality of the Green's function analytical method, in this case two heat sources as described in Section 2 were applied, one heat source to represent the shoulder and one to represent the pin of the tool. The parameters of the proposed heat source model, for both the pin and shoulder components, are shown in Table 2; note all heat source parameters are given in mm unless stated otherwise. The steel tool had pin and shoulder widths of $5\ mm$ and $12.7\ mm$ respectively; as such the values of a and c_f for the pin and shoulder were set to be $5\ mm$ and $\frac{12.7}{2}\ mm$ respectively such that the heat generation from the shoulder occurred at its mid-plane. The value of c_r was chosen to be slightly higher to account for hot material deposited behind the tool as it travelled. The only remaining parameters to fit then are b and f .

The predicted temperatures for the three thermocouples in closest proximity to the tool are shown in Fig. 7. Chao et al. simulated the FSW

process using the finite element method. The measured and simulated peak temperatures for the TC_{top} , TC_{middle} and TC_{bottom} locations are shown in Table 3. Table 3 also shows the peak temperature for the same locations computed in this work using the volumetric heat flux and solved analytically.

It should then be noted that the performance of the analytical approach with applied volumetric heat source terms for the pin and shoulder arguably performs as well, if not better, than the finite element model of Chao at predicting the peak temperatures close to the friction stir weld. In the analytical solution computed in this work, insulating boundary conditions are imposed at B , D and L . In the experiment a backing plate was attached at the $y = D$ location. A Dirichlet boundary condition could be applied here, with a -1^n factor in the y -component of the Green's function, and may give a better approximation of the temperature field in this case.

5. Discussion

There are enormous advantages to computing the temperature field using the analytical solution technique; the availability of a representative heat source model, coupled with a time dependent efficiency term, permits the transient thermal field induced in a finite domain to be computed far more rapidly than is possible with numerical methods such as the finite element method. The temperature field computed in this manner is free from numerical uncertainties introduced by the spatial and temporal discretisation. The disadvantage of the analytical solution technique by Green's functions is that the

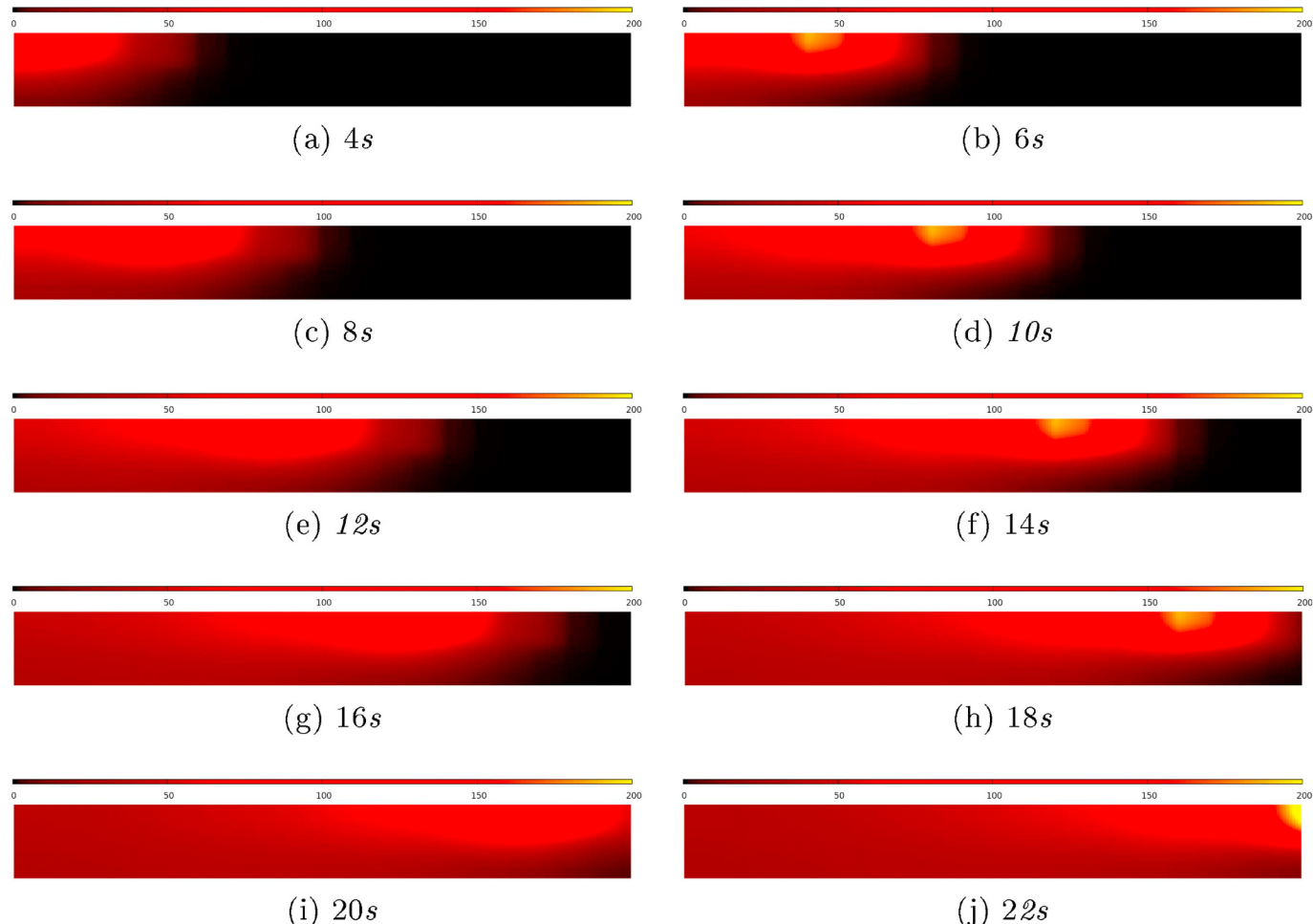


Fig. 6. Cross section through the computational domain at the welding joint showing the thermal response due to the volumetric FSW heat source flux distribution with a periodically varying heat input to the simulated work-piece.

Table 2

Heat source parameters for the 'hot' and 'cold' weld for comparison with the literature.

Case	Heat ^a Source	<i>a</i>	<i>b</i>	<i>c_r</i>	<i>c_f</i>	<i>y_i</i>	<i>d_g</i>	<i>b_g</i>	<i>f</i>	<i>Pη^b</i>
'hot'	<i>q_p</i>	5	0.2	8	5	1	5.2	102	0.45	620
	<i>q_s</i>	$\frac{12.7}{2}$	3.0	12.7	$\frac{12.7}{2}$	0	1	102	$1 - f_{pin}$	620
'cold'	<i>q_p</i>	5	0.2	8	5	1	5.2	102	0.5	762
	<i>q_s</i>	$\frac{12.7}{2}$	3.0	12.7	$\frac{12.7}{2}$	0	1	102	$1 - f_{pin}$	762

^a Subscripts refer to pin and shoulder components.

^b Units of power are $J\ s^{-1}$

method of images formulation of the boundary conditions means that only orthogonal boundary conditions may be considered; this orthogonality problem is not encountered with FSW, or laser and electron beam welding, when a square-but configuration is employed, so these processes are amenable to analytical solutions.

The presented example applications show how a wide variety of time depend heat input rates may be accounted for. Although further validation of the volumetric heat source is required, the comparison with experimental results presented in the literature shows the temperatures computed analytically due to the proposed model are in good agreement with those measured experimentally. If this new heat source model is shown to perform well with further validation cases it offers huge advantages, given its ability to simulate time dependent heat input rates and to calculate the induced temperature field analytically. The advantages of the presented solution procedure are not only in reduced computational cost but also relate to confidence in predicted temperatures.

The advantages of the proposed heat source model and analytical solution for the transient temperature field are:

- More representative than a surface flux based approach.
- Extremely computationally efficient.
- Accounts for time dependent heat input.
- Fitted parameters are related to the pin and shoulder geometry.

The disadvantages of the proposed model are:

- Flow field is not explicitly solved for, as a result it is not expected that the predicted temperatures will be as accurate as those predicted by a fully coupled CFD approach.

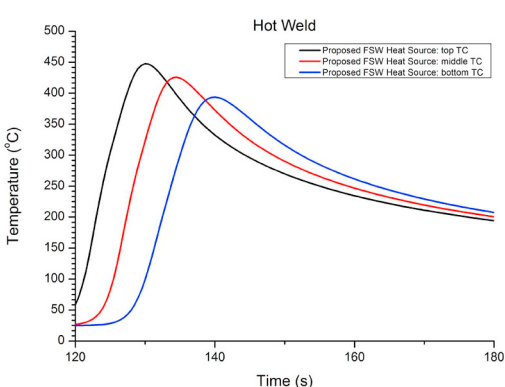
Table 3

Peak temperatures recorded by the thermocouples closest to the weld-line compared with numerical simulation by Chao et al. and the analytical solution with volumetric heat source presented in this work [34].

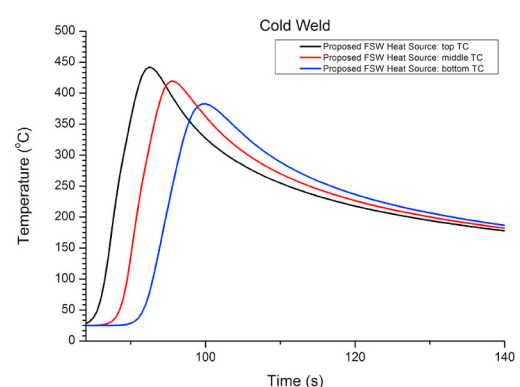
Case	Thermocouple Location	Experimental Peak Temperature	Chao Simulated Peak Temperature	Analytically Computed Peak Temperature
'hot weld'	(107,2,295.5)	~ 445 °C	~ 440 °C	447 °C
	(107,4,305)	~ 425 °C	~ 405 °C	426 °C
	(107, D, 314.5)	~ 340 °C	~ 390 °C	387 °C
'cold weld'	(107,2,295.5)	~ 440 °C	~ 430 °C	339 °C
	(107,4,305)	~ 430 °C	~ 390 °C	418 °C
	(107, D, 314.5)	~ 300 °C	~ 370 °C	383 °C

As mentioned previously the heat source is based on the difference between two Gaussian distributions, while the fitted parameters in this model are based on the geometry of the tool and as such are not arbitrary. Some preliminary checks have been carried out in this work, but it is also helpful to consider what may happen in extreme circumstances to see if the model behaves as expected. For example, as $(d_g - y_i)$ is increased, representing the tool penetrating further into the component, the predicted temperature at the base of the component is increased, as expected. As discussed, two heat sources may be considered, representing the tool and shoulder respectively; if the shoulder component is removed, as was the case in the sinusoidal and ramping examples, representing perhaps the application of the tool without a pin, the volumetric heat source behaves as expected, with peak values of heat transfer assigned at locations corresponding to the radius of the pin.

The current work does not concentrate on the heat arising from the FSW tool explicitly. The aim of the presented model is to find the temperature field around a known heat source. This heat source has a complex spatial distribution as shown in Fig. 2, and multiple heat sources may be superimposed, as long as $\sum_{n=1}^N f_n = 1$, where N is the number of heat sources utilised. In addition, the heat input in the model is permitted to vary with time, therefore if the material slip rate and heat transfer rate to the material can be extracted from experimental data, the presented modelling approach could account for these effects. In other words the heat flux can be precisely modified when the analytical results are compared with the experimental data. This comparison is logical when the accuracy of analytical results is validated by other methods such as finite element methods and CFD.



(a) Predicted temperature at the TC_{top} , TC_{middle} and TC_{bottom} for the 'hot' weld.



(b) Predicted temperature at the TC_{top} , TC_{middle} and TC_{bottom} for the 'cold' weld.

Fig. 7. Predicted temperature response at the thermocouple locations computed analytically for the 'hot' and 'cold' FSW of AA2195 Aluminium.

6. Conclusions

In the present work time dependent heat input rates are accounted for in an analytical solution for the transient temperature field induced in a finite domain subject to a novel volumetric heat source representing heat generation in the FSW process. Examples of predicted temperature fields due to this volumetric heat source are presented in order to demonstrate that the predictions of the model are accurate.

The performance of the model and analytical solution scheme were compared against two cases presented in the literature; good agreement was achieved between predicted peak temperatures close to the weld line and those measured experimentally. The method permits the transient thermal field induced in a finite domain, due to a distributed heat source which varies in space as well as time, to be computed analytically in a computationally efficient manner free from numerical uncertainties. The analytical basis of the model offers a drastic reduction in solution times. The model is also extremely versatile, since limitless variations on the time dependence of the heat transfer rate from the tool to the work-piece may be incorporated. The method may be used to represent sudden losses of power in the welding process, thus

offering the capability to assess the development of microstructure and the induced thermal strains.

To the authors knowledge this is the first time a volumetric heat source of this kind has been used to simulate the FSW process. It is also the first time the temporal effects of the dwell periods on the temperature field have been explicitly simulated and their effects on the transient temperature investigated. An exact solution to the transient temperature field induced in a finite domain due to a proposed novel doughnut-like volumetric heat source, varying in space and time, was presented. The analytical solution presented in this work may be easily extended to incorporate alternative boundary conditions where appropriate.

Acknowledgements

The authors wish to acknowledge financial support from the Engineering and Physical Sciences Research Council (EPSRC) through the NNUMAN programme grant in nuclear manufacturing (Grant No. EP/J021172/1).

Appendix A. Derivation of Volumetric Heat Source

The functional form of the distribution was chosen to be the difference between two Gaussian functions in a given direction. Consider the x -coordinate to have the form: $e^{-3\left(\frac{x}{P+r}\right)^2} - e^{-3\left(\frac{x}{r}\right)^2}$. Now it is required to find the maxima in this distribution, this is done by differentiating the function and equating to zero in order to find the peak locations, $\frac{\partial}{\partial x} \left(e^{-3\left(\frac{x}{P+r}\right)^2} - e^{-3\left(\frac{x}{r}\right)^2} \right) = \frac{-3x^2}{r^2} - \frac{6e^{-\frac{3x^2}{r^2}}x}{r^2} = 0$. Therefore the location of the maxima in the distributions occurs at $x = b_g \pm \frac{rP\sqrt{\log[P^2]}}{\sqrt{-3+3P^2}}$ where b_g is the origin of the distribution. Now the value of P can be chosen appropriately as per Figure A.8.

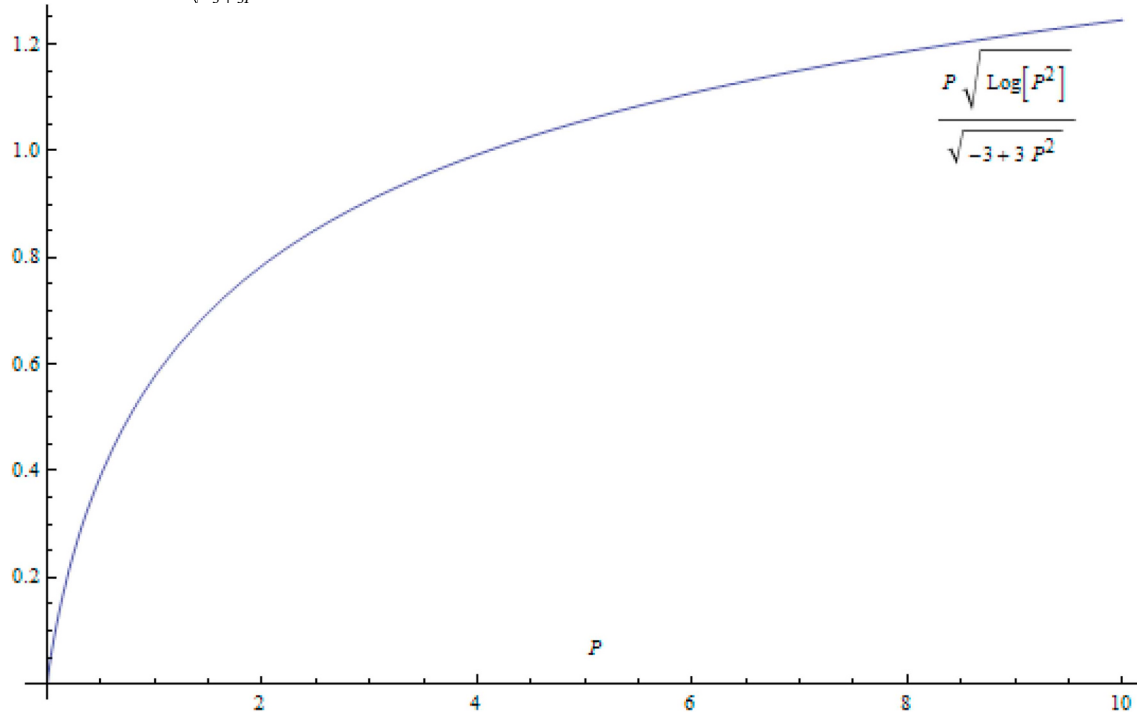


Fig. A.8. Choosing the value of the parameter P appropriately.

The value of P is chosen as $\pi/3$. Therefore the peak flux value occurs at $x = b_g \pm \frac{r(\pi/3)\sqrt{\ln[(\pi/3)^2]}}{\sqrt{-3+3(\pi/3)^2}} = b_g \pm rk_p$ where k_p is a constant and has a value

of $\frac{\frac{\pi}{3}\sqrt{\ln\left[\frac{\pi^2}{9}\right]}}{\sqrt{3\left(\frac{\pi^2}{9}\right)-3}} \simeq 0.59071$. It is desirable to specify the peak location of heat flux generation in the distribution, as such, the denominator in the exponent

for each spatial component is r/k_p . To ensure continuity and heat accountancy the quadrants must be integrated and matched at the quadrant boundaries. The quadrants below the base of the cylinder, ahead and trailing the $\xi = 0$ origin have the form as shown in Equation (A.1) and Equation (A.2) respectively. The two quadrants above the base of the cylinder have the form shown in Equation (A.3) for the portion ahead of the heat source location and Equation (A.4) for the column component $\xi < 0$.

$$q_{fb}(x,y,\xi) = Q_{0f \text{ base}} \begin{cases} e^{-3 \times \left(\left(\frac{x-b_g}{(\pi/3)\left(\frac{a}{k_p}\right)} \right)^2 + \left(\frac{y-d_g}{b} \right)^2 + \left(\frac{\xi}{(\pi/3)\left(\frac{c_f}{k_p}\right)} \right)^2 \right)} \\ - e^{-3 \times \left(\left(\frac{x-b_g}{\left(\frac{a}{k_p}\right)} \right)^2 + \left(\frac{y-d_g}{b} \right)^2 + \left(\frac{\xi}{\left(\frac{c_f}{k_p}\right)} \right)^2 \right)} \end{cases} \quad (\text{A.1})$$

$$q_{rb}(x,y,\xi) = Q_{0r \text{ base}} \begin{cases} e^{-3 \times \left(\left(\frac{x-b_g}{(\pi/3)\left(\frac{a}{k_p}\right)} \right)^2 + \left(\frac{y-d_g}{b} \right)^2 + \left(\frac{\xi}{(\pi/3)\left(\frac{c_r}{k_p}\right)} \right)^2 \right)} \\ - e^{-3 \times \left(\left(\frac{x-b_g}{\left(\frac{a}{k_p}\right)} \right)^2 + \left(\frac{y-d_g}{b} \right)^2 + \left(\frac{\xi}{\left(\frac{c_r}{k_p}\right)} \right)^2 \right)} \end{cases} \quad (\text{A.2})$$

$$q_{fc}(x,y,\xi) = Q_{0f \text{ column}} \begin{cases} e^{-3 \times \left(\left(\frac{x-b_g}{(\pi/3)\left(\frac{a}{k_p}\right)} \right)^2 + \left(\frac{\xi}{(\pi/3)\left(\frac{c_f}{k_p}\right)} \right)^2 \right)} \\ - e^{-3 \times \left(\left(\frac{x-b_g}{\left(\frac{a}{k_p}\right)} \right)^2 + \left(\frac{\xi}{\left(\frac{c_f}{k_p}\right)} \right)^2 \right)} \end{cases} \quad (\text{A.3})$$

$$q_{rc}(x,y,\xi) = Q_{0r \text{ column}} \begin{cases} e^{-3 \times \left(\left(\frac{x-b_g}{(\pi/3)\left(\frac{a}{k_p}\right)} \right)^2 + \left(\frac{\xi}{(\pi/3)\left(\frac{c_r}{k_p}\right)} \right)^2 \right)} \\ - e^{-3 \times \left(\left(\frac{x-b_g}{\left(\frac{a}{k_p}\right)} \right)^2 + \left(\frac{\xi}{\left(\frac{c_r}{k_p}\right)} \right)^2 \right)} \end{cases} \quad (\text{A.4})$$

In order to find the values of $Q_{0f \text{ base}}$, $Q_{0r \text{ base}}$, $Q_{0f \text{ column}}$ and $Q_{0r \text{ column}}$ these distributions must be integrated with some knowledge of the matching at the boundaries that will be performed. Consider the leading component of the base quadrant as shown in Equation (A.1), integrating over the region this quadrant operates:

$$\int_0^\infty \int_{d_g}^\infty \int_{-\infty}^\infty q_{fb}(x,y,\xi) dx dy d\xi = \frac{Q_{0f \text{ base}} abc_f \pi^{3/2} (\pi^2 - 9)}{108 \times \sqrt{3} k_p^2} = R_l$$

where R_l is a parameter that must be found to ensure the heat distributions match at the boundaries. Therefore the expression for $Q_{0f \text{ base}}$ is given in Equation (A.5).

$$Q_{0f \text{ base}} = \frac{108 \times R_l \times \sqrt{3} k_p^2}{abc_f \pi^{3/2} (\pi^2 - 9)} \quad (\text{A.5})$$

Similar expressions for $Q_{0r \text{ base}}$, $Q_{0f \text{ column}}$ and $Q_{0r \text{ column}}$ are found in the same way with appropriate integration limits. These expressions are shown in Equations A.6, A.7 and A.8 respectively.

$$Q_{0r \text{ base}} = \frac{108 \times R_2 \times \sqrt{3} k_p^2}{abc_r \pi^{3/2} (\pi^2 - 9)} \quad (\text{A.6})$$

$$Q_{0f \text{ column}} = \frac{54 \times R_3 \times k_p^2}{ac_f \pi (d_g - y_i) (\pi^2 - 9)} \quad (\text{A.7})$$

$$Q_{0r \text{ column}} = \frac{54 \times R_4 \times k_p^2}{ac_f \pi (d_g - y_i) (\pi^2 - 9)} \quad (\text{A.8})$$

R_1 , R_2 , R_3 and R_4 now must be found by matching the flux distributions of the four quadrants at the origin of the reference frame. At the point $(b_g, d_g, 0)$ the distributions in the four quadrants are equal. $q_{fb}(x,y,\xi) = q_{rb}(x,y,\xi) = q_{fc}(x,y,\xi) = q_{rc}(x,y,\xi)$. Expressions for the R terms may then be found in terms of one another, this fact and knowing that the total spatial integral must sum to unity to ensure all heat generation is accounted for allows their computation as shown in Equation (A.9).

$$\begin{aligned} R_1 + \left(\frac{c_r}{c_f} \times R_1 \right) + \left(\frac{108\sqrt{3}k_p^2}{ab\pi^{3/2}(-9+\pi^2)\times c_f} \times \frac{a\pi(-9+\pi^2)\times c_f \times (d_g - y_i)}{54k_p^2} \times R_1 \right) \\ + \left(\frac{108\sqrt{3}k_p^2}{ab\pi^{3/2}(-9+\pi^2)\times c_f} \times \frac{a\pi(-9+\pi^2)\times c_r \times (d_g - y_i)}{54k_p^2} \times R_1 \right) = 1 \end{aligned} \quad (\text{A.9})$$

Solving this equation gives an expression for R_1 as $R_1 = \frac{b c_f}{(c_f + c_r)\left(b + 2\sqrt{\frac{3}{\pi}}(d_g - y_l)\right)}$. Similar expressions may then be found for the remaining quadrants which are shown in Equation (A.10).

$$\begin{aligned} R_1 &= \frac{b c_f}{(c_f + c_r)\left(b + 2\sqrt{\frac{3}{\pi}}(d_g - y_l)\right)} R_2 = \frac{b c_r}{(c_f + c_r)\left(b + 2\sqrt{\frac{3}{\pi}}(d_g - y_l)\right)} \\ R_3 &= \frac{6 c_f (d_g - y_l)}{(c_f + c_r)(6(d_g - y_l) + b\sqrt{3\pi})} R_4 = \frac{6 c_r (d_g - y_l)}{(c_f + c_r)(6(d_g - y_l) + b\sqrt{3\pi})} \end{aligned} \quad (\text{A.10})$$

Now the final form of the flux distribution is known and the integral over all space will return unity.

References

- [1] Z.Y. Ma, Friction stir processing technology: a review, *Metall. Mater. Trans.* 39 (3) (2008) 642–658.
- [2] H.R. Shercliff, M.J. Russel, a Taylor, T.L. Dickerson, Microstructural modelling in friction stir welding of 2000 series aluminium alloys, *Mec. Ind.* 6 (01) (2005) 25–35.
- [3] W.M. Thomas, E.D. Nicholas, Friction stir welding for the transportation industries, *Mater. Des.* 18 (4) (1997) 269–273.
- [4] F. Hannard, S. Castin, E. Maire, R. Mokso, T. Pardoën, A. Simar, Ductilization of aluminium alloy 6056 by friction stir processing, *Acta Mater.* 130 (Supplement C) (2017) 121–136.
- [5] A. Tongne, C. Desrayaud, M. Jahazi, E. Feulvach, On material flow in Friction Stir Welded Al alloys, *J. Mater. Process. Technol.* 239 (Supplement C) (2017) 284–296.
- [6] C.R. Feng, R.W. Fonda, H.N. Jones, Shoulder contact and gas shielding in titanium friction stir welds, *Sci. Technol. Weld. Join.* 19 (1) (2014) 2–8.
- [7] L. Shi, C.S. Wu, Transient model of heat transfer and material flow at different stages of friction stir welding process, *J. Manuf. Process.* 25 (Supplement C) (2017) 323–339.
- [8] R. Rai, A. De, H.K.D.H. Bhadeshia, T. DebRoy, Review: friction stir welding tools, *Sci. Technol. Weld. Join.* 16 (4) (2011) 325–342.
- [9] Diogo Mariano Neto, Neto Pedro, Numerical modeling of friction stir welding process: a literature review, *Int. J. Adv. Manuf. Technol.* 65 (1) (mar 2013) 115–126.
- [10] Hao Wu, Ying-Chun Chen, David Strong, Phil Prangnell, Stationary shoulder FSW for joining high strength aluminum alloys, *J. Mater. Process. Technol.* 221 (jul 2015) 187–196.
- [11] H.B. Schmidt, J.H. Hattel, Thermal modelling of friction stir welding, *Scripta Mater.* 58 (5) (mar 2008) 332–337.
- [12] H. Schmidt, J. Hattel, Modelling heat flow around tool probe in friction stir welding, *Sci. Technol. Weld. Join.* 10 (2) (2005) 176–186.
- [13] Yongxian Huang, Yuming Xie, Xiangchen Meng, Zongliang Lv, Jian Cao, Numerical design of high depth-to-width ratio friction stir welding, *J. Mater. Process. Technol.* 252 (Supplement C) (2018) 233–241.
- [14] R. Nandan, G.G. Roy, T.J. Liener, T. DebRoy, Three-dimensional heat and material flow during friction stir welding of mild steel, *Acta Mater.* 55 (3) (2007) 883–895.
- [15] Paul A. Colegrove, Hugh R. Shercliff, 3-Dimensional CFD modelling of flow round a threaded friction stir welding tool profile, *J. Mater. Process. Technol.* 169 (2) (2005) 320–327.
- [16] Yihua Xiao, Haifei Zhan, Yuantong Gu, Qinghua Li, Modeling heat transfer during friction stir welding using a meshless particle method, *Int. J. Heat Mass Tran.* 104 (Supplement C) (2017) 288–300.
- [17] X.K. Zhu, Y.J. Chao, Numerical simulation of transient temperature and residual stresses in friction stir welding of 304L stainless steel, *J. Mater. Process. Technol.* 146 (2) (feb 2004) 263–272.
- [18] C.M. Chen, R. Kovacevic, Finite element modeling of friction stir welding-thermal and thermomechanical analysis, *Int. J. Mach. Tool Manufact.* 43 (13) (oct 2003) 1319–1326.
- [19] H. Schmidt, J. Hattel, J. Wert, An analytical model for the heat generation in friction stir welding, *Model. Simulat. Mater. Sci. Eng.* 12 (1) (2004) 143–157.
- [20] Jesper Henri Hattel, Henrik Nikolaj Blicher Schmidt, C. Tutum, Thermomechanical modelling of friction stir welding, *Proceedings of the 8th International Conference on Trends in Welding Research*, 2009, pp. 1–6.
- [21] Gaoqiang Chen, Han Li, Guoqing Wang, Zhiqiang Guo, Shuai Zhang, Qilei Dai, Xibo Wang, Gong Zhang, Qingyu Shi, Effects of pin thread on the in-process material flow behavior during friction stir welding: a computational fluid dynamics study, *Int. J. Mach. Tool Manufact.* 124 (Supplement C) (2018) 12–21.
- [22] A.F. Hasan, C.J. Bennett, P.H. Shipway, S. Cater, J. Martin, A numerical methodology for predicting tool wear in Friction Stir Welding, *J. Mater. Process. Technol.* 241 (Supplement C) (2017) 129–140.
- [23] Paul A. Colegrove, Hugh R. Shercliff, Rudolf Zettler, Model for predicting heat generation and temperature in friction stir welding from the material properties, *Sci. Technol. Weld. Join.* 12 (4) (2007) 284–297.
- [24] Mohammad Haghpansahi, Solaleh Salimi, Pouya Bahemmat, Sadaf Sima, 3-D transient analytical solution based on Green's function to temperature field in friction stir welding, *Appl. Math. Model.* 37 (24) (2013) 9865–9884.
- [25] Nab Raj Roshyara, Gerald Wilhelm, Ulrich Semmler, Arnd Meyer, Approximate analytical solution for the temperature field in welding, *Metall. Mater. Trans. B* 42 (6) (jul 2011) 1253–1273.
- [26] T.F. Flint, J.A. Francis, M.C. Smith, A.N. Vasileiou, Semi-analytical solutions for the transient temperature fields induced by a moving heat source in an orthogonal domain, *Int. J. Therm. Sci.* 123 (jan 2018) 140–150.
- [27] X.K. Zhu, Y.J. Chao, Effects of temperature-dependent material properties on welding simulation, *Comput. Struct.* 80 (11) (2002) 967–976.
- [28] Gaoqiang Chen, Qingxian Ma, Shuai Zhang, Jianjun Wu, Gong Zhang, Qingyu Shi, Computational fluid dynamics simulation of friction stir welding: a comparative study on different frictional boundary conditions, *J. Mater. Sci. Technol.* 34 (1) (jan 2018) 128–134.
- [29] J.A. Goldak, M.J. Bibby, A. Chakravarti, A new finite element model for welding heat sources, *Metall. Trans. B* 15 (1984) 299–305.
- [30] C.S. Wu, H.G. Wang, Y.M. Zhang, A new heat source model for keyhole plasma arc welding in FEM analysis of the temperature profile, *Welding Res.* (2006) 284–291 (December).
- [31] T.F. Flint, J.A. Francis, M.C. Smith, J. Balakrishnan, Extension of the double-ellipsoidal heat source model to narrow-groove and keyhole weld configurations, *J. Mater. Process. Technol.* 246 (2017) 123–135.
- [32] K.D. Cole, A. Haji-Sheikh, James V. Beck, Bahman Litkouhi, *Heat Conduction Using Greens Functions*, 2 edition, Taylor and Francis, 2011.
- [33] Thomas F. Flint, John A. Francis, John R. Yates, Analytical solutions of the transient thermal field induced in finite bodies with insulating and convective boundary conditions subjected to a welding heat source, *Conf. Proc.: Struct. Mech. Reactor Technol.* 22 (2013) San Francisco.
- [34] Yuh J. Chao, X. Qi, W. Tang, Heat transfer in friction stir welding-experimental and numerical studies, *J. Manuf. Sci. Eng.* 125 (1) (2003) 138–145.